

Mixed QCD-EW corrections to vector-boson production

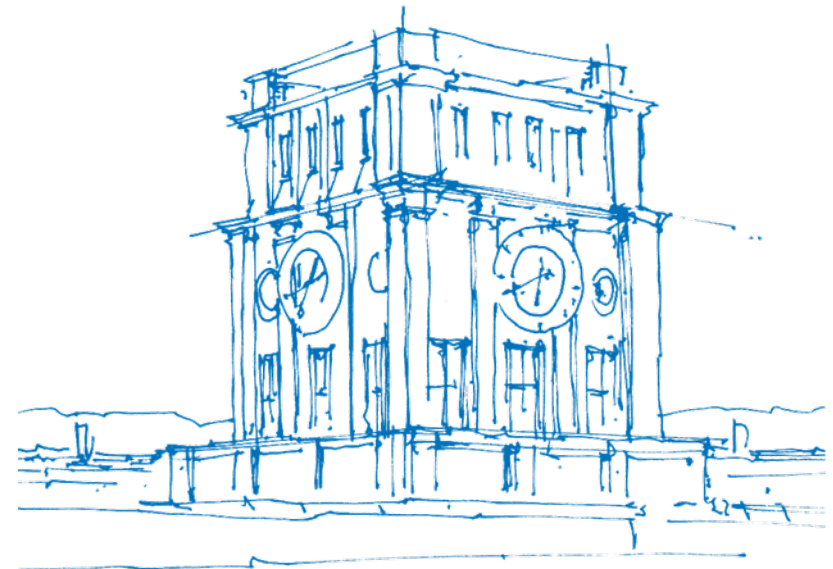
In collaboration with: A. Behring, F. Buccioni, F. Caola, M. Jaquier, K. Melnikov, R. Röntsch

Based on: 1909.08428, 2005.10221, 2009.10386, 2103.02671

Maximilian Delto

ISSP at EMFCSC

21th of June 2022



TUM Uhrenturm

QCD computations have reached N3LO

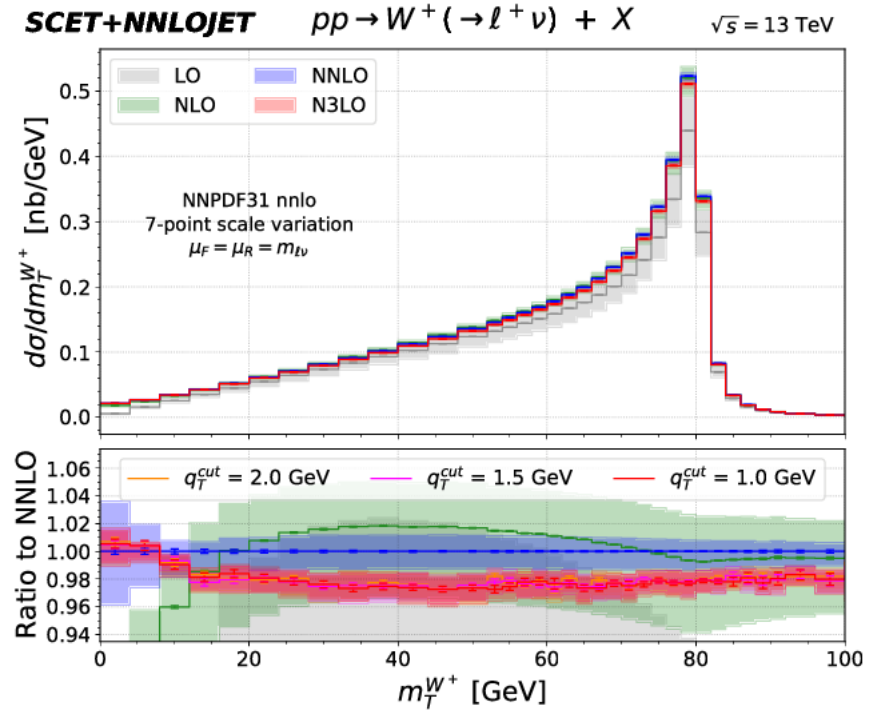
Fully-differential description of color-singlet production at the LHC has recently reached N3LO in perturbative QCD.

⇒ Higgs production [Chen et al. '21]

⇒ Drell-Yan [Chen et al. '22]

Parametrically, $\alpha_s^3 \sim \alpha_s \alpha$.
 $\alpha_s(M_Z) \sim 0.1$, $\alpha \sim 1/100$

These computations are vital for precise studies at the LHC.



[Chen et al. '22]

M_W as a precision test

electroweak fits

$$M_W^2(1 - M_W^2/M_Z^2) = \frac{\pi\alpha}{\sqrt{2}G_F}(1 + \Delta r)$$

$$M_W = 80354 \pm 7 \text{ MeV [Gfitter'18]}$$

$$M_W = 80359 \pm 5 \text{ MeV [HEPfit'21]}$$

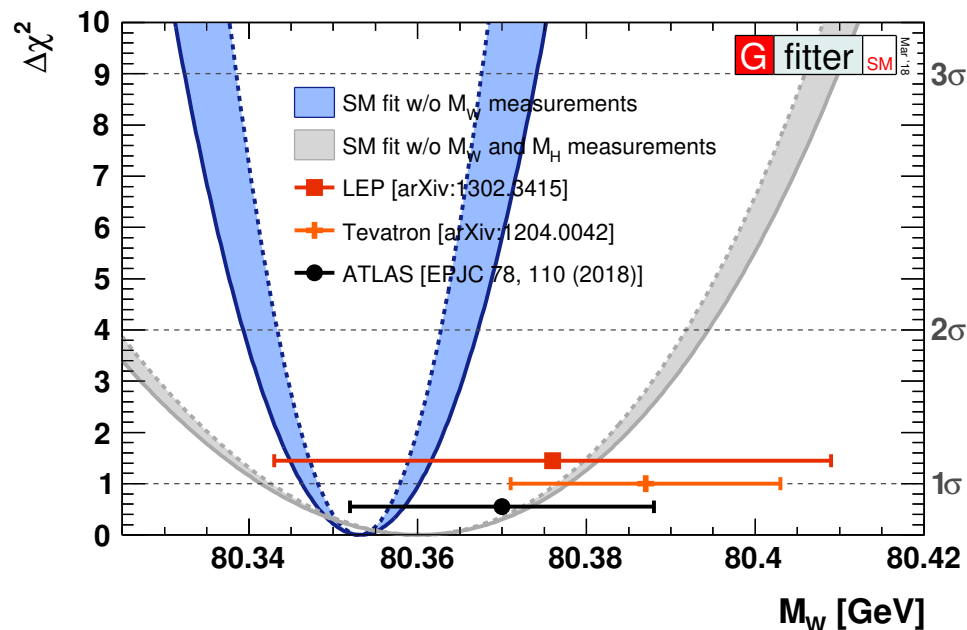
recent direct measurements

$$\text{[ATLAS '17]} : 80370 \pm 7_{\text{stat}} \pm 11_{\text{sys}} \pm 14_{\text{mod}} \text{ MeV}$$

$$\text{[LHCb '21]} : 80354 \pm 23_{\text{stat}} \pm 10_{\text{exp}} \pm 17_{\text{th}} \pm 9_{\text{pdf}} \text{ MeV}$$

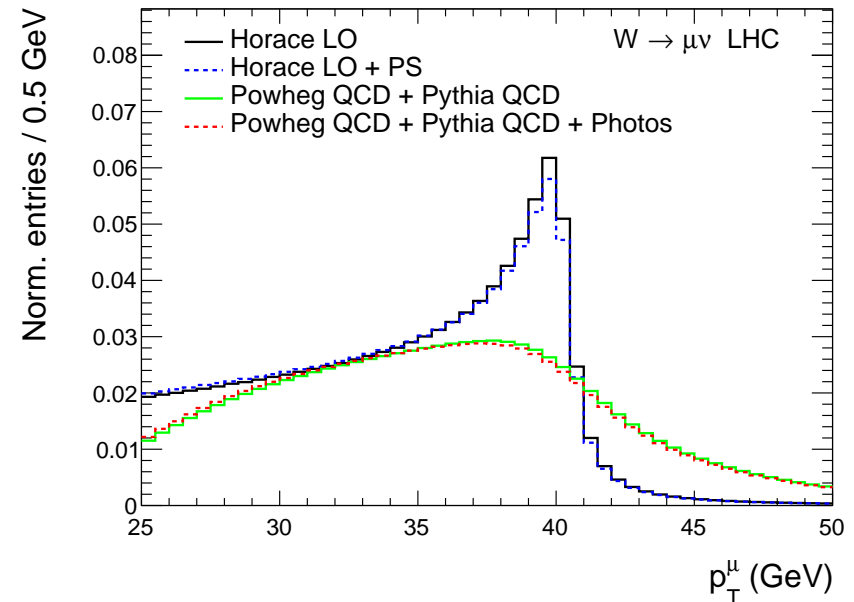
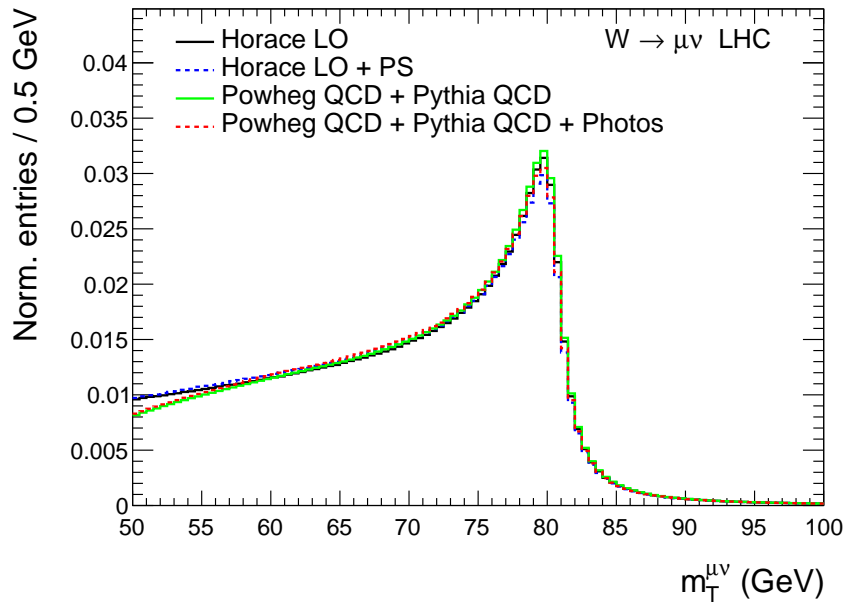
$$\text{[CDF '22]} : 80433.5 \pm 6.4_{\text{stat}} \pm 6.9_{\text{sys}} \text{ MeV}$$

comparison



Measurement of M_W (at hadron colliders)

- through leptonic decay $pp \rightarrow W^* \rightarrow \ell \bar{\nu}$
 - partonic center-of-mass energy \hat{s} not known, neutrino momentum p_ν cannot be measured
- \Rightarrow measurements use shape of distributions in p_\perp^ℓ and m_\perp^W



[Calame et al. '16]

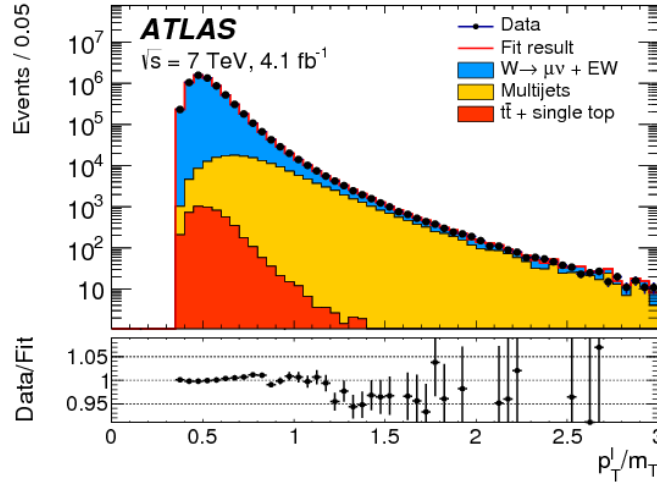
- $m_\perp^W = \sqrt{2p_\perp^\ell p_\perp^{\text{miss}}(1 - \cos \phi_{\ell, \text{miss}})} \leq M_W$
- W -boson width, pile-up
- see [Smith, van Neerven, Vermaseren '83]

- at LO: $p_\perp^\ell \leq m_W/2$
- perturbative corrections

Measurement of M_W (at hadron colliders)

template fit

collinear factorization [Collins,Soper,Sterman '88]



$$8/80'000 = 0.01\%$$

$$\sigma = \sum_{i,j} \int_0^1 dx_1 dx_2 \underbrace{f_i(x_1) f_j(x_2)}_{\mathcal{O}(1\%)} \overbrace{\sigma_{ij}(x_1, x_2)}^{\mathcal{O}(1\%)} + \mathcal{O}\left(\frac{\Lambda_{\text{QCD}}^2}{Q^2}\right)$$

$\Rightarrow p_{\perp}^W$ spectrum can not be predicted to required precision.

- experimental analyses use Z-boson data to predict p_{\perp}^W distribution
- hence, measurement is sensitive to effects that distinguish between W and Z
- these include PDFs, massive-quark effects, NLO EW and NNLO QCD-EW corrections

Vector-boson production at $\mathcal{O}(\alpha_s \alpha)$

- p_{\perp}^W/p_{\perp}^Z distribution is dominated by the on-shell production of vector bosons

$$d\sigma|_{\alpha_s \alpha} = \left| \underbrace{\text{production}}_{\alpha_s} \otimes \underbrace{\text{decay}}_{\alpha} \right|^2 + \left| \underbrace{\text{production}}_{\alpha_s \alpha} \right|^2 + \mathcal{O}\left(\frac{\Gamma_V}{M_V}\right)$$

[Dittmaier et al. '14 '16] [Behring et al. '19 '20]

- full, off-shell process $pp \rightarrow \ell \bar{\ell}$ was completed recently [Bonciani et al. '21] [Buccioni et al. '22]

Infrared divergences at NLO

$$\left. \frac{d\sigma}{d\mathbf{O}} \right|_{\alpha_s} = 2 \Re \left[\underbrace{\left[\text{Diagram 1} \right]}_{\sim 1/\epsilon^2} \times \left[\text{Diagram 2} \right] \right] \mathcal{F}_0 d\Phi_X + \left| \left[\text{Diagram 3} \right] + \left[\text{Diagram 4} \right] \right|^2 \mathcal{F}_0^{(1)} d\Phi_{X+g} + d\sigma^{gq} + d\sigma^{\text{pdf}}$$

- cross-section is *finite* for arbitrary “infrared-safe” observable \mathcal{F}

Infrared divergences at NLO

$$\left. \frac{d\sigma}{d\mathbf{O}} \right|_{\alpha_s} = 2 \Re \left[\underbrace{\left[\text{Diagram 1} \right]}_{\sim 1/\epsilon^2} \times \left[\text{Diagram 2} \right] \right] \mathcal{F}_0 d\Phi_X + \left| \left[\text{Diagram 3} \right] + \left[\text{Diagram 4} \right] \right|^2 \mathcal{F}_0^{(1)} d\Phi_{X+g} + d\sigma^{gq} + d\sigma^{\text{pdf}}$$

- cross-section is *finite* for arbitrary “infrared-safe” observable \mathcal{F}
- individually, soft and collinear divergences arise from

Infrared divergences at NLO

$$\left. \frac{d\sigma}{d\mathbf{O}} \right|_{\alpha_s} = 2 \Re \left[\underbrace{\left[\text{Diagram 1} \right]}_{\sim 1/\epsilon^2} \times \left[\text{Diagram 2} \right] \right] \mathcal{F}_0 d\Phi_X + \left| \left[\text{Diagram 3} \right] + \left[\text{Diagram 4} \right] \right|^2 \mathcal{F}_0^{(1)} d\Phi_{X+g} + d\sigma^{gq} + d\sigma^{\text{pdf}}$$

The diagrams represent Feynman diagrams for NLO corrections. Diagram 1 shows a loop with a gluon (curly line) and a quark (straight line) with momenta p_1 and p_2 . Diagram 2 shows a quark line with momenta p_1 and p_2 and a gluon line. Diagram 3 and 4 show quark lines with momenta p_1 and p_2 and a gluon line with momentum k_4 .

- cross-section is *finite* for arbitrary “infrared-safe” observable \mathcal{F}
- individually, soft and collinear divergences arise from
 - **loop integrals** in virtual corrections

Infrared divergences at NLO

$$\frac{1}{p_1 \cdot k_4} \sim \frac{1}{E_1 E_4 (1 - \cos \theta_{14})}$$

$$\left. \frac{d\sigma}{d\mathbf{O}} \right|_{\alpha_s} = 2 \Re \left[\underbrace{\left[\text{Diagram 1} \right]}_{\sim 1/\epsilon^2} \times \left[\text{Diagram 2} \right] \mathcal{F}_0 d\Phi_X + \left| \text{Diagram 3} + \text{Diagram 4} \right|^2 \mathcal{F}_0^{(1)} d\Phi_{X+g} + d\sigma^{gq} + d\sigma^{\text{pdf}} \right]$$

Diagram 1: A loop diagram with incoming momenta p_1 and p_2 , a loop with a gluon and a quark, and an outgoing gluon. Diagram 2: A tree-level diagram with incoming momenta p_1 and p_2 , and an outgoing quark. Diagram 3: A tree-level diagram with incoming momenta p_1 and p_2 , and two outgoing gluons, one of which is labeled k_4 . Diagram 4: A tree-level diagram with incoming momenta p_1 and p_2 , and two outgoing gluons, one of which is labeled k_4 .

- cross-section is *finite* for arbitrary “infrared-safe” observable \mathcal{F}
- individually, soft and collinear divergences arise from
 - **loop integrals** in virtual corrections
 - **phase-space integration** over on-shell momenta of final-state partons in real-emission corrections

Infrared divergences at NLO

$$\frac{1}{p_1 \cdot k_4} \sim \frac{1}{E_1 E_4 (1 - \cos \theta_{14})}$$

$$\left. \frac{d\sigma}{dO} \right|_{\alpha_s} = 2 \Re \left[\underbrace{\left[\text{Diagram 1} \right]}_{\sim 1/\epsilon^2} \times \left[\text{Diagram 2} \right] \mathcal{F}_O d\Phi_X + \left| \text{Diagram 3} + \text{Diagram 4} \right|^2 \mathcal{F}_O^{(1)} d\Phi_{X+g} + d\sigma^{gq} + d\sigma^{\text{pdf}}$$

Diagram 1: A loop diagram with incoming momenta p_1 and p_2 , a loop with a gluon and a quark, and an outgoing gluon. Diagram 2: A tree-level diagram with incoming momenta p_1 and p_2 , and an outgoing gluon. Diagram 3: A tree-level diagram with incoming momenta p_1 and p_2 , and two outgoing gluons with momenta k_4 and k_4 . Diagram 4: A tree-level diagram with incoming momenta p_1 and p_2 , and two outgoing gluons with momenta k_4 and k_4 .

- cross-section is *finite* for arbitrary “infrared-safe” observable \mathcal{F}
- individually, soft and collinear divergences arise from
 - **loop integrals** in virtual corrections
 - **phase-space integration** over on-shell momenta of final-state partons in real-emission corrections
- need to be regulated, extracted and cancelled

Infrared divergences at NLO

$$\frac{1}{p_1 \cdot k_4} \sim \frac{1}{E_1 E_4 (1 - \cos \theta_{14})}$$

$$\left. \frac{d\sigma}{d\mathbf{O}} \right|_{\alpha_s} = 2 \Re \left[\underbrace{\left[\text{Diagram 1} \right]}_{\sim 1/\epsilon^2} \times \left[\text{Diagram 2} \right] \mathcal{F}_0 d\Phi_X + \left| \text{Diagram 3} + \text{Diagram 4} \right|^2 \mathcal{F}_0^{(1)} d\Phi_{X+g} + d\sigma^{gq} + d\sigma^{\text{pdf}} \right]$$

Diagram 1: A loop diagram with incoming momenta \$p_1\$ and \$p_2\$, a loop with a gluon and a quark, and an outgoing gluon. Diagram 2: A tree-level diagram with incoming momenta \$p_1\$ and \$p_2\$, and an outgoing gluon. Diagram 3: A tree-level diagram with incoming momenta \$p_1\$ and \$p_2\$, and two outgoing gluons, one of which is labeled \$k_4\$. Diagram 4: A tree-level diagram with incoming momenta \$p_1\$ and \$p_2\$, and two outgoing gluons, one of which is labeled \$k_4\$.

- cross-section is *finite* for arbitrary “infrared-safe” observable \mathcal{F}
- individually, soft and collinear divergences arise from
 - **loop integrals** in virtual corrections
 - **phase-space integration** over on-shell momenta of final-state partons in real-emission corrections
- need to be regulated, extracted and cancelled
- only then can the limit $\epsilon \rightarrow 0$ be taken prior to numerical simulation

slicing / subtraction

Infrared divergences at NLO

$$\frac{1}{p_1 \cdot k_4} \sim \frac{1}{E_1 E_4 (1 - \cos \theta_{14})}$$

$$\left. \frac{d\sigma}{dO} \right|_{\alpha_s} = 2 \Re \left[\underbrace{\left[\text{Diagram 1} \right]}_{\sim 1/\epsilon^2} \times \left[\text{Diagram 2} \right] \right] \mathcal{F}_O d\Phi_X + \left| \left[\text{Diagram 3} \right] + \left[\text{Diagram 4} \right] \right|^2 \mathcal{F}_O^{(1)} d\Phi_{X+g} + d\sigma^{gq} + d\sigma^{\text{pdf}}$$

$\sim 1/\epsilon^2$

- cross-section is *finite* for arbitrary “infrared-safe” observable \mathcal{F}
- individually, soft and collinear divergences arise from
 - **loop integrals** in virtual corrections
 - **phase-space integration** over on-shell momenta of final-state partons in real-emission corrections
- need to be regulated, extracted and cancelled
- only then can the limit $\epsilon \rightarrow 0$ be taken prior to numerical simulation

\Rightarrow *slicing* and *subtraction* schemes
are used to define contributions that are individually finite



$$\left. d\sigma \right|_{\alpha_s} = d\sigma_{X+1} + d\sigma_X$$

Infrared subtraction at NLO

- general idea is to subtract and add back matrix elements that approximate singular behavior

$$d\sigma^{q\bar{q}}(d = 4 - 2\epsilon) = \underbrace{(d\sigma^r - d\tilde{\sigma}^r)}_{\text{regulated term}} \Big|_{d=4} + \underbrace{d\tilde{\sigma}^r(\epsilon)}_{\text{subtraction term}}$$

- pole cancellation

$$\lim_{\epsilon \rightarrow 0} \left[d\sigma^{\text{pdf}} + d\sigma^v(\epsilon) + d\tilde{\sigma}^r(\epsilon) \right] = \text{finite}$$

- example for soft-regulated emission of a gluon

$$d\sigma^{q\bar{q}} = \left\{ \left| \begin{array}{c} p_1 \\ \text{gluon } k_4 \\ p_2 \end{array} \right|^2 + \left| \begin{array}{c} p_1 \\ \text{gluon } k_4 \\ p_2 \end{array} \right|^2 - \frac{2g_s^2 C_F (p_1 \cdot p_2)}{(p_1 \cdot k_4)(p_2 \cdot k_4)} \left| \begin{array}{c} p_1 \\ \text{gluon } k_4 \\ p_2 \end{array} \right|^2 \right\} d\Phi_{V+g} \\ + \underbrace{\left(\int [dk_4] \frac{2g_s^2 C_F (p_1 \cdot p_2)}{(p_1 \cdot k_4)(p_2 \cdot k_4)} \right)}_{\sim 1/\epsilon^2} \times \left(\left| \begin{array}{c} p_1 \\ \text{gluon } k_4 \\ p_2 \end{array} \right|^2 d\Phi_V \right)$$

- NB similar formula for remaining collinear divergence

Quark emission at NNLO QCD-EW

$$|\mathcal{A}_{ud \rightarrow W^+ dd}|^2 \Big|_{\mathcal{O}(\alpha_s \alpha)} \supset \text{[QCD diagram]} \times \left[\text{[EW diagrams]} \right]^\dagger$$

The diagram shows a quark line (u1) emitting a W boson (W) and a gluon (g). The gluon splits into two quarks (d4, d5). The EW diagrams show the W boson interacting with a quark line (u1) via a loop involving a photon (gamma) or Z boson, which then splits into two quarks (d4, d5).

- only triple-collinear divergence $p_2 \parallel k_4 \parallel k_5$ due to continuous quark line

$$\begin{aligned} d\sigma_{ud \rightarrow W^+ dd}^{\text{rr}} &= \langle [dk_4][dk_5] (I - \hat{\mathcal{C}}_2) F_{\text{LM}}(1_u, 2_d, W^+; 4_d, 5_d) \rangle && \leftarrow \text{fully regulated} \\ &+ \langle [dk_4][dk_5] \hat{\mathcal{C}}_2 F_{\text{LM}}(1_u, 2_d, W^+; 4_d, 5_d) \rangle && \leftarrow \text{subtraction term} \end{aligned}$$

- integrated triple-collinear subtraction terms were computed in the context of NNLO QCD corrections [\[MD, Melnikov '19\]](#), results can be re-used here

$$\begin{aligned} &\langle [dk_4][dk_5] \mathcal{C}_2 F_{\text{LM}}(1_u, 2_d, W^+; 4_d, 5_d) \rangle \\ &\sim \alpha_s \alpha \times \int_0^1 dz \left[\underbrace{\frac{f_1(z)}{\varepsilon}}_{\text{pole cancellation}} + \underbrace{f_0(z)}_{\text{physical XS}} \right] \left\langle \frac{C_F Q_d^2 F_{\text{LM}}(1_u, z \cdot 2_{\bar{d}})}{z} \right\rangle, \quad z = \frac{E_2 - E_4 - E_5}{E_2} \end{aligned}$$

Impact on the M_W measurement at the LHC

- goal: construct “simple” observable for M_W^{exp} that makes use of both the $p_{\ell,Z}^\perp$ distribution and the precisely measured Z-boson mass

→ define normalized average momentum as

$$\left\langle p_{\ell,V}^\perp \theta \left[p_{\ell,V}^\perp - p_{\text{cut}}^\perp \right] \right\rangle = \frac{\int \theta^{\text{cut}} p_{\ell,V}^\perp \times \frac{d\sigma_V}{dp_{\ell,V}^\perp} dp_{\ell,V}^\perp}{\int \theta^{\text{cut}} d\sigma_V} = M_V \times f \left(\frac{p_{\text{cut}}^\perp}{M_V} \right)$$

→ define observable M_W^{exp} as

$$M_W^{\text{exp}} = \frac{\left\langle p_{\ell,W}^\perp \right\rangle^{\text{exp}}}{\left\langle p_{\ell,Z}^\perp \right\rangle^{\text{exp}}} M_Z C_{\text{th}}, \quad C_{\text{th}} = \frac{M_W}{M_Z} \frac{\left\langle p_{\ell,Z}^\perp \right\rangle^{\text{th}}}{\left\langle p_{\ell,W}^\perp \right\rangle^{\text{th}}}$$

Impact on the M_W measurement at the LHC

- updated theoretical description shifts extracted value of M_W

$$\delta M_W^{\text{exp}} = \left[\frac{\delta \langle p_{\ell,Z}^\perp \rangle^{\text{th}}}{\langle p_{\ell,Z}^\perp \rangle^{\text{th}}} - \frac{\delta \langle p_{\ell,W}^\perp \rangle^{\text{th}}}{\langle p_{\ell,W}^\perp \rangle^{\text{th}}} \right] M_W^{\text{exp}}$$

	<u>inclusive</u>	ATLAS cuts	tuned cuts
NLO EW	<u>1 MeV</u>	3 MeV	−3 MeV
NNLO QCD-EW	<u>−7 MeV</u>	−17 MeV	−1 MeV

$$\delta \langle p_{\ell,W}^\perp \rangle^{\text{th}} / \langle p_{\ell,W}^\perp \rangle^{\text{th}} \times M_W^{\text{exp}} \sim \mathcal{O}(30 - 50) \text{ MeV}$$

⇒ large cancellation by one order of magnitude

⇒ sensitive to cuts

Impact on the M_W measurement at the LHC

- updated theoretical description shifts extracted value of M_W

$$\delta M_W^{\text{exp}} = \left[\frac{\delta \langle p_{\ell,Z}^\perp \rangle^{\text{th}}}{\langle p_{\ell,Z}^\perp \rangle^{\text{th}}} - \frac{\delta \langle p_{\ell,W}^\perp \rangle^{\text{th}}}{\langle p_{\ell,W}^\perp \rangle^{\text{th}}} \right] M_W^{\text{exp}}$$

	inclusive	<u>ATLAS cuts</u>	tuned cuts
NLO EW	1 MeV	<u>3 MeV</u>	−3 MeV
NNLO QCD-EW	−7 MeV	<u>−17 MeV</u>	−1 MeV

ATLAS $p_{\ell,V}^\perp$ -cuts:

→ $p_{\text{cut},Z}^\perp = 25 \text{ GeV}$

→ $p_{\text{cut},W}^\perp = 30 \text{ GeV}$

⇒ moves average momentum in decays of the lighter W boson towards higher values

Impact on the M_W measurement at the LHC

- updated theoretical description shifts extracted value of M_W

$$\delta M_W^{\text{exp}} = \left[\frac{\delta \langle p_{\ell,Z}^\perp \rangle^{\text{th}}}{\langle p_{\ell,Z}^\perp \rangle^{\text{th}}} - \frac{\delta \langle p_{\ell,W}^\perp \rangle^{\text{th}}}{\langle p_{\ell,W}^\perp \rangle^{\text{th}}} \right] M_W^{\text{exp}}$$

	inclusive	ATLAS cuts	<u>tuned cuts</u>
NLO EW	1 MeV	3 MeV	<u>−3 MeV</u>
NNLO QCD-EW	−7 MeV	−17 MeV	<u>−1 MeV</u>

find tuned value for $p_{\text{cut},W}^\perp$ such that $C_{\text{th}}^{\text{LO}} = 1$ with $p_{\text{cut},Z}^\perp = 25$ GeV

$\Rightarrow p_{\text{cut},W}^\perp = 25.44$ GeV (instead of $p_{\text{cut},W}^\perp = 30$ GeV)

Conclusion

- fully-differential description of QCD-EW corrections to on-shell vector-boson production
 - regularisation of infrared singularities
 - analytic computation of integrated subtraction terms
 - (on-shell form factor $pp \rightarrow W$, including two-loop master integrals with two internal masses)

⇒ QCD-EW corrections were estimated
to shift the measurement of M_W by up to **−17 MeV**

Outlook

⇒ this result warrants further studies,
which incorporate all relevant details of experimental analyses

Backup

Breakdown LHCb uncertainties

Source	Size [MeV]
Parton distribution functions	9
Theory (excl. PDFs) total	17
Transverse momentum model	11
Angular coefficients	10
QED FSR model	7
Additional electroweak corrections	5
Experimental total	10
Momentum scale and resolution modelling	7
Muon ID, trigger and tracking efficiency	6
Isolation efficiency	4
QCD background	2
Statistical	23
Total	32

[LHCb '21]

Breakdown CDF uncertainties

Table 2. Uncertainties on the combined M_W result.

Source	Uncertainty (MeV)
Lepton energy scale	3.0
Lepton energy resolution	1.2
Recoil energy scale	1.2
Recoil energy resolution	1.8
Lepton efficiency	0.4
Lepton removal	1.2
Backgrounds	3.3
p_T^Z model	1.8
p_T^W/p_T^Z model	1.3
Parton distributions	3.9
QED radiation	2.7
W boson statistics	6.4
Total	9.4

[CDF '22]